Hepatocellular carcinoma (HCC) is the third leading cause of cancer death worldwide.[16] Although the cellular origin of HCC is unclear,[17,18] HCC has heterogeneous pathologies and genetic/genomic profiles,[19] suggesting that HCC can initiate in different cell lineages.[20] The liver is considered as a maturational lineage system similar to that in the bone marrow.[21] Experimental evidence indicates that certain forms of hepatic stem cells (HpSCs), present in human livers of all donor ages, are multipotent and can give rise to hepatoblasts,[22,23] which are, in turn, bipotent progenitor cells that can progress either into hepatocytic or biliary lineages.[22,24] α-fetoprotein (AFP) is one of the earliest markers detected in the liver bud specified from the ventral foregut,[25,26] but its expression has been found only in hepatoblasts and to a lesser extent in committed hepatocytic progenitors, not in later lineages or in normal human HpSC.[22] Recent studies also have indicated that EpCAM is a biomarker for HpSC because it is expressed in HpSCs and hepatoblasts.[22–24]

We recently identified a novel HCC classification system based on EpCAM and AFP status.[27] Gene expression profiles revealed that EpCAM$^+$ AFP$^+$ HCC (referred to as *HpSC-HCC*) has progenitor features with poor prognosis, whereas EpCAM$^-$ AFP$^-$ HCC (referred to as *mature hepatocyte-like HCC*; MH-HCC) have adult hepatocyte features with good prognosis. Wnt/β-catenin signaling, a critical player for maintaining embryonic stem cells,[28] is activated in EpCAM$^+$ AFP$^+$ HCC, and EpCAM is a direct transcriptional target of Wnt/β-catenin signaling.[29] Moreover, EpCAM$^+$ AFP$^+$ HCC cells are more sensitive to β-catenin inhibitors than EpCAM$^-$ HCC cells in vitro.[29] Interestingly, a heterogeneous expression of EpCAM and AFP was observed in clinical tissues, a feature that may be attributed to the presence of a subset of CSCs. In this study, we have confirmed that EpCAM$^+$ HCC cells are highly invasive and tumorigenic, and have activated Wnt/β-catenin signaling. We also show a crucial role of EpCAM in the maintenance of hepatic CSCs. Our data shed new light on the pathogenesis of HCC and may open new avenues for therapeutic interventions for targeting hepatic CSCs.

Materials and Methods

Clinical Specimens

HCC samples were obtained with informed consent from patients who underwent radical resection at the Liver Cancer Institute of Fudan University, Eastern Hepatobiliary Surgery Institute, and the Liver Disease Center of Kanazawa University Hospital, and the study was approved by the institutional review boards of the respective institutes. The microarray data from clinical specimens are available publicly (GEO accession number, GSE5975).[27] Array data from a total of 156 HCC cases (155 hepatitis B virus [HBV]-positive) corresponding to 2 subtypes of HCC (ie, HpSC-HCC and MH-HCC), were used to search for HpSC-HCC–associated genes (Supplementary Table 1; see supplementary material online at www.gastrojournal.org). A total of 79 formalin-fixed and paraffin-embedded HCC samples were used for immunohistochemistry (IHC) analyses (Supplementary Table 2; see supplementary material online at www.gastrojournal.org), 56 of which also were used in a recent study.[30] The classification of HpSC-HCC and MH-HCC was based on previously described criteria.[27]

Cell Cultures and Sorting

Human liver cancer cell lines (HuH1 and HuH7) were derived from Health Science Research Resources Bank (JCRB0199 and JCRB0403, respectively) and routinely cultured as previously described.[31] Normal human MHs, provided by the University of Pittsburgh through Liver Tissue Cell Distribution System, were cultured as previously described.[32] Human HpSCs were isolated from fetal livers and cultured in Kubota and Reid's[33] medium as previously described. Wnt10B conditioned medium was prepared as described.[34] Embryonic stem cell culture medium was prepared using Knockout Dulbecco's modified Eagle medium supplemented with 18% of Serum Replacement (Invitrogen, Carlsbad, CA). The pTOP-FLASH and pFOP-FLASH luciferase constructs were described previously.[29] BIO and MeBIO were generous gifts from Ali Brivanlou (The Rockefeller University, New York, NY). For isolating single cell–derived colonies to determine whether heterogeneity is an intrinsic property of EpCAM$^+$ cells, HuH1 and HuH7 cells were resuspended and plated as a single cell per well in 96-well plates. A total of 192 single cells were plated successfully. The clones that grew well were selected 2 weeks after seeding and used for immunofluorescence (IF) analysis. The 5-fluorouracil (5-FU) stock (2 mg/mL; Sigma, St Louis, MO), was prepared in distilled water. Fluorescence-activated cell sorting (FACS) and magnetic-activated cell sorting (MACS) analyses were used to isolate EpCAM$^+$ HCC cells (Supplementary materials; see supplementary Materials and Methods online at www.gastrojournal.org).

Clonogenicity, Spheroid Formation, Invasion, Quantitative Reverse Transcription–Polymerase Chain Reaction, and IHC Assays

For colony formation assays, 2000 EpCAM$^+$ or EpCAM$^-$ cells were seeded in 6-well plates after FACS. After 10 days of culture, cells were fixed by 100% methanol and stained with methylene blue. For spheroid assays, single-cell suspensions of 1000 EpCAM$^+$ or EpCAM$^-$ cells were seeded in 6-well Ultra-Low Attachment Microplates (Corning, Corning, NY) after FACS. The number of spheroids was measured 14 days after seeding. Invasion assays were performed using BD BioCoat Matrigel Matrix Cell Culture Inserts and Control Inserts (BD Biosciences, San Jose, CA) essentially as pre-

viously described.[31] Reverse transcription-polymerase chain reaction and IHC assays are described in detail in the supplementary materials (see supplementary material online at www.gastrojournal.org).

Tumorigenicity in NOD/SCID Mice

Six-week-old NOD/SCID mice (NOD/NCrCRl-*Prkdc*^{scid}) were purchased from Charles River (Charles River Laboratories, Inc, Wilmington, MA). The protocol was approved by the National Cancer Institute–Bethesda Animal Care and Use Committee. Cells were suspended in 200 μL of Dulbecco's modified Eagle medium and Matrigel (1:1), and a subcutaneous injection was performed. The size and incidence of subcutaneous tumors were recorded. For histologic evaluation, tumors were formalin-fixed, paraffin-embedded or embedded directly in OCT compound (Sakura Finetek, Torrance, CA) and stored at −80°C.

RNA Interference

A small interfering RNA (siRNA) specific to *TACSTD1* (SI03019667) and a control siRNA (1022076) were designed and synthesized by Qiagen (Qiagen, Valencia, CA). Transfection was performed using Lipofectamine 2000 (Invitrogen), according to the manufacturer's instructions. A total of 200 nmol/L of siRNA duplex was used for each transfection.

Statistical Analyses

The class comparison and gene clustering analyses were performed as previously described.[30] The canonic pathway analysis was performed using Ingenuity Pathways Analysis (v5.5; Ingenuity Systems, Redwood City, CA). The association of HCC subtypes and clinicopathologic characteristics was examined using either the Mann–Whitney *U* test or the chi-square test. Student *t* tests were used to compare various test groups assayed by colony formation, spheroid formation, or invasion assays. The Kaplan–Meier survival analysis was performed to compare patient survival or tumorigenicity.

Results

A Poor Prognostic HCC Subtype With Molecular Features of HpSC

We re-evaluated the gene expression profiles that were uniquely associated with 2 recently identified prognostic subtypes of HCC (ie, HpSC-HCC and MH-HCC), using a publicly available microarray dataset of 156 HCC cases (GEO accession number: GSE5975). Sixty cases were defined as HpSC-HCC with a poor prognosis and 96 cases were defined as MH-HCC with a good prognosis, based on EpCAM and AFP status.[27] A class-comparison analysis with univariate *t* tests and a global permutation test (1000×) yielded 793 genes that were expressed differentially between HpSC-HCC and MH-HCC ($P < .001$). Hierarchical cluster analyses revealed 2 main gene clusters that were up-regulated (cluster A; 455 genes) or down-regulated (cluster B; 338 genes) in HpSC-HCC (Figure 1*A*). Pathway analysis indicated that the enriched genes in cluster A were associated significantly with known stem cell signaling pathways such as transforming growth factor-β, Wnt/β-catenin, PI3K/Akt, and integrin ($P < .01$) (Figure 1*B*). In contrast, genes in cluster B were associated significantly with mature hepatocyte functions such as xenobiotic metabolism, complement system, and coagulation system ($P < .01$). Noticeably, known HpSC markers such as *KRT19* (CK19), *TACSTD1* (EpCAM), *AFP*, *DKK1*, *DLK1*, and *PROM1* (CD133) were up-regulated significantly in HpSC-HCC, whereas known liver maturation markers such as *UGT2B7* and *CYP3A4* were expressed more abundantly in MH-HCC (Figure 1*C* and Supplementary Tables 3 and 4; see supplementary material online at www.gastrojournal.org). Kaplan–Meier survival analysis revealed that HpSC-HCC patients had a significantly shorter survival than MH-HCC patients ($P = .036$) (Figure 1*D*). Consistently, HpSC-HCC patients had a high frequency of macroscopic and microscopic portal vein invasion (Figure 1*E*).

However, IHC analyses of an additional 79 HCC cases revealed that among 24 HpSC-HCC cases, EpCAM staining was very heterogeneous with a mixture of EpCAM$^+$ and EpCAM$^-$ tumor cells in each tumor (Figure 1*F*, *left panel*). Noticeably, many of the EpCAM$^+$ tumor cells were located at the invasion border zones and often were disseminated at the invasive front (*black arrows*). IF analysis revealed that HCC cells located at the invasive front co-expressed EpCAM, CK19, and AFP (Figure 1*F*, *right panels*). Noticeably, HpSC-HCC patients were significantly younger than MH-HCC patients (Supplementary Tables 1 and 2; see supplementary material online at www.gastrojournal.org). Enrichment of EpCAM$^+$ AFP$^+$ tumor cells at the tumor-invasive front suggested their involvement in HCC invasion and metastasis.

Isolation and Characterization of EpCAM$^+$ Cells in HCC

The results described earlier suggest that HpSC-HCC may be organized in a hierarchical fashion in which EpCAM$^+$ tumor cells act as stem-like cells with an ability to differentiate into EpCAM$^-$ tumor cells. To test this hypothesis, we first evaluated the expression pattern of 7 hepatic stem/maturation markers (EpCAM, CD133, CD90, CK19, Vimentin, Hep-Par1, and β-catenin) in 6 HCC cell lines (Figure 2*A*). All 3 AFP$^+$ cell lines (HuH1, HuH7, and Hep3B) expressed EpCAM, CD133, and cytoplasmic/nuclear β-catenin, whereas the other 3 AFP$^-$ cell lines (SK–Hep-1, HLE, and HLF) did not, consistent with the microarray data. Interestingly, AFP$^+$ cell lines had no CD90$^+$ cell population, which recently was identified as hepatic CSCs,[35] whereas AFP$^-$ cell lines had such a population. Consistent with the IF data, FACS analysis showed that AFP$^+$ cell lines had a subpopulation of

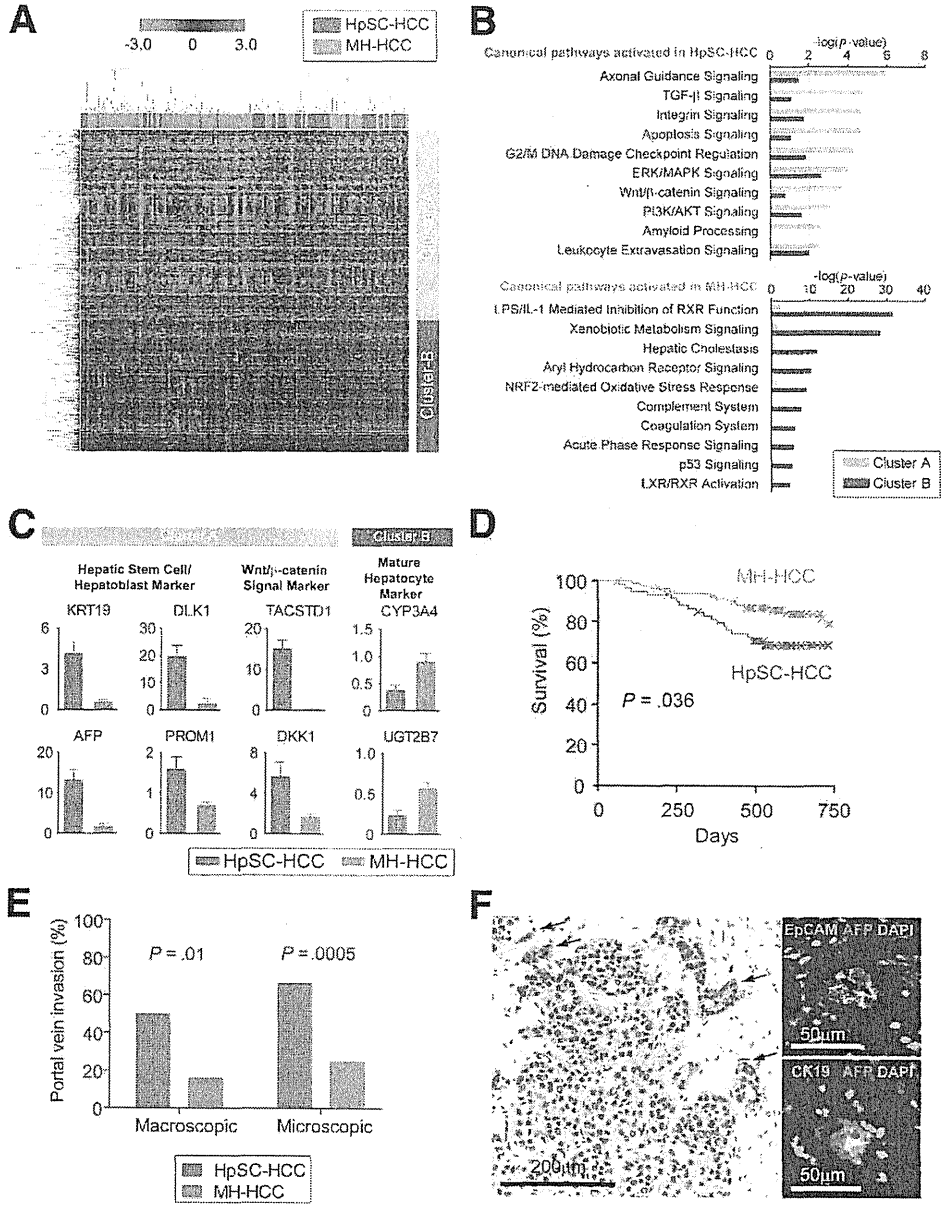

Figure 1. HpSC–HCC represents a subset of invasive HCCs with CSC features. (*A*) Hierarchical cluster analysis based on 793 HpSC–HCC–coregulated genes in 156 HCC cases. Each cell in the matrix represents the expression level of a gene in an individual sample. Red and green cells depict high and low expression levels, respectively, as indicated by the scale bar. (*B*) Pathway analysis of HpSC–HCC–coregulated genes. The top 10 canonical signaling pathways activated in cluster A (*upper panel*) or cluster B (*lower panel*) with statistical significance ($P < .01$) are shown. (*C*) Expression patterns of well-known HpSC and MH markers in each HCC subtype as analyzed by microarray. (*D*) Kaplan–Meier survival analysis of the cases used for array analysis. (*E*) Frequency of macroscopic and microscopic portal vein invasion in HpSC-HCC and MH-HCC used for IHC. (*F*) Representative images of EpCAM, AFP, and CK19 staining in HpSC–HCC samples analyzed by IHC and IF. EpCAM staining illustrates heterogeneous expression of EpCAM in HpSC-HCC (*left panel*). EpCAM$^+$ cells were disseminated in the invasive border (*left panel black arrows*) with expression of AFP (*right top panel*) and CK19 (*right bottom panel*).

EpCAM$^+$ and CD133$^+$, but no CD90$^+$ cells, whereas AFP$^-$ cell lines had a subpopulation of CD90$^+$ cells but no EpCAM$^+$ or CD133$^+$ cells (Figure 2*B*). These data indicate that HpSC-HCC and MH-HCC cell lines have distinct stem cell marker expression patterns, and EpCAM as well as CD133 may be hepatic CSC markers specifically in HpSC-HCC.

We selected 2 human HCC cell lines (HuH1 and HuH7) to isolate EpCAM$^+$ cells because both lines were heterogeneous in EpCAM, AFP, CK19, and β-catenin expression (Figure 2*A* and *B* and Supplementary Figure 1*A*; see supplementary material online at www.gastrojournal.org).[29] We successfully enriched EpCAM$^+$ and EpCAM$^-$ populations from HuH7 cells by FACS, with more than 80% purity in EpCAM$^+$ cells and more than 90% purity in EpCAM$^-$ cells 1 day after sorting (Figure 3*A*). Similar results were obtained when the purity check was performed immediately after sorting (data not shown). EpCAM$^+$ cells also were positive for CK19 and β-catenin (Figure 3*B* and Supplementary Figure 1*B*; see supplementary material online at www.gastrojournal.org) and most were AFP$^+$ (data not shown). In contrast, EpCAM$^-$ cells were negative for these markers but positive for HepPar1, a monoclonal antibody specific to hepatocytes (Figure 3*B*). Consistent with the microarray data described earlier, the levels of *TACSTD1*, *MYC*, and *hTERT* (known HpSC markers) were increased significantly in EpCAM$^+$ HuH7 cells, whereas the levels of *UGT2B7* and *CYP3A4*

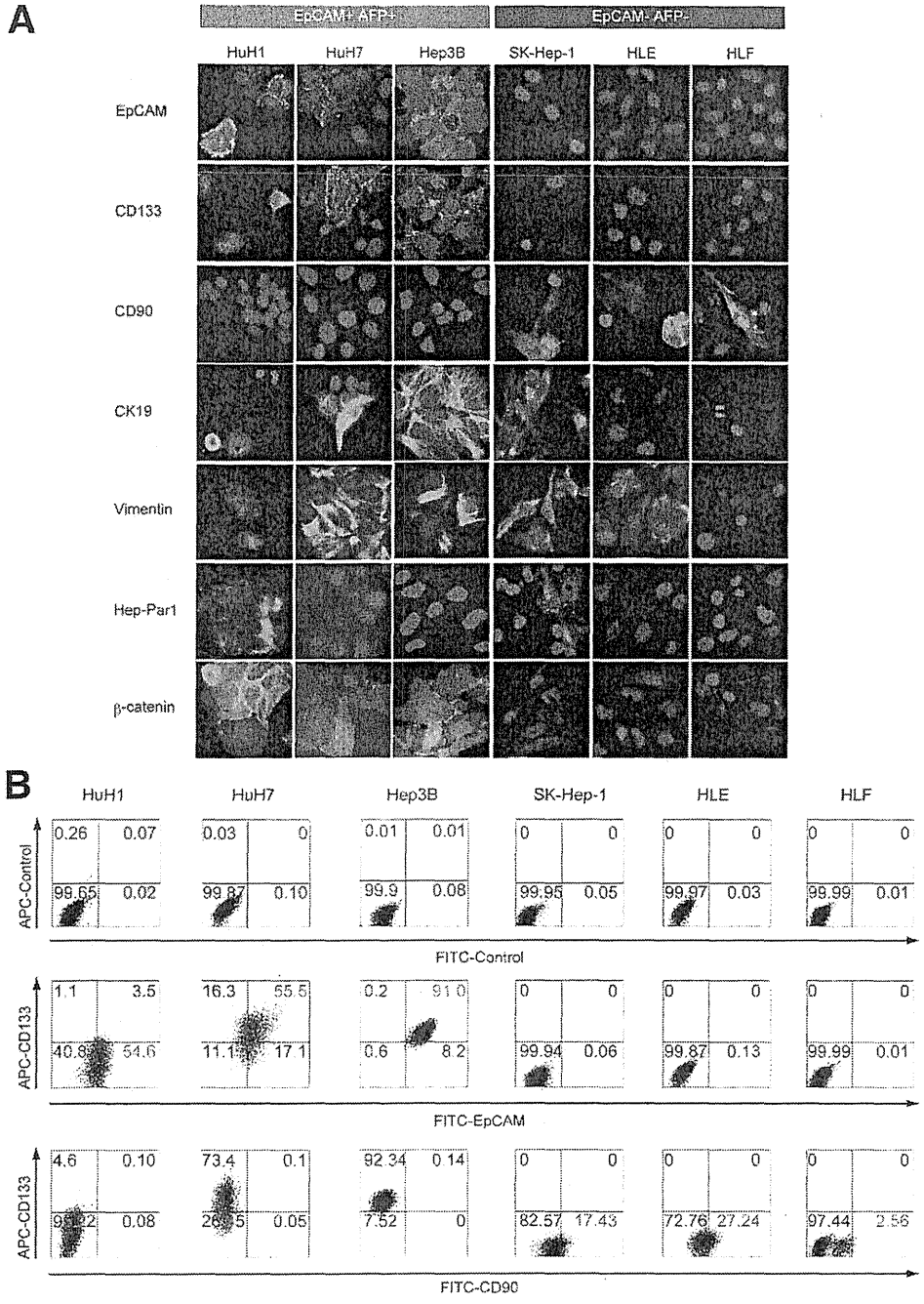

Figure 2. Characterization of hepatic stem cell marker expression in HCC cell lines. (*A*) IF analysis of 6 HCC cell lines (EpCAM$^+$ AFP$^+$ cell lines: HuH1, HuH7, and Hep3B; EpCAM$^-$ AFP$^-$ cell lines: SK-Hep-1, HLE, and HLF) stained with anti-EpCAM, anti-CD133, anti-CD90, anti-CK19, anti-Vimentin, anti–Hep-Par1, and anti–β-catenin antibodies. (*B*) FACS analysis of 6 HCC cell lines stained with anti-EpCAM, anti-CD133, and anti-CD90 antibodies.

(known mature hepatocyte markers) were significantly higher in EpCAM$^-$ HuH7 cells (Figure 3*C*, *left upper panel*). This expression pattern was reminiscent of human HpSC cells (Figure 3*C*, *left lower panel*). Similar results were obtained from HuH1 cells (data not shown). We also compared gene expression patterns of isolated HuH1, HuH7, MH, and HpSC cells using the TaqMan Human Stem Cell Pluripotency Array (Applied Biosystems, Foster City, CA) containing 96 selected human stem cell–related genes. Although a differential expression pattern of stem cell–related genes was evident among HpSC, EpCAM$^+$ HuH1, and EpCAM$^+$ HuH7 cells, the EpCAM$^+$ HCC cells were related more closely to HpSC cells whereas EpCAM$^-$ HCC cells were related more closely to diploid adult mature hepatocytes (Figure 3*C*, *right panel*; and Supplementary Figure 1*C*; see supplementary material online at www.gastrojournal.org). Thus, it appeared that EpCAM$^+$ HCC cells had a gene expression pattern that is related more closely to HpSC than EpCAM$^-$ HCC cells.

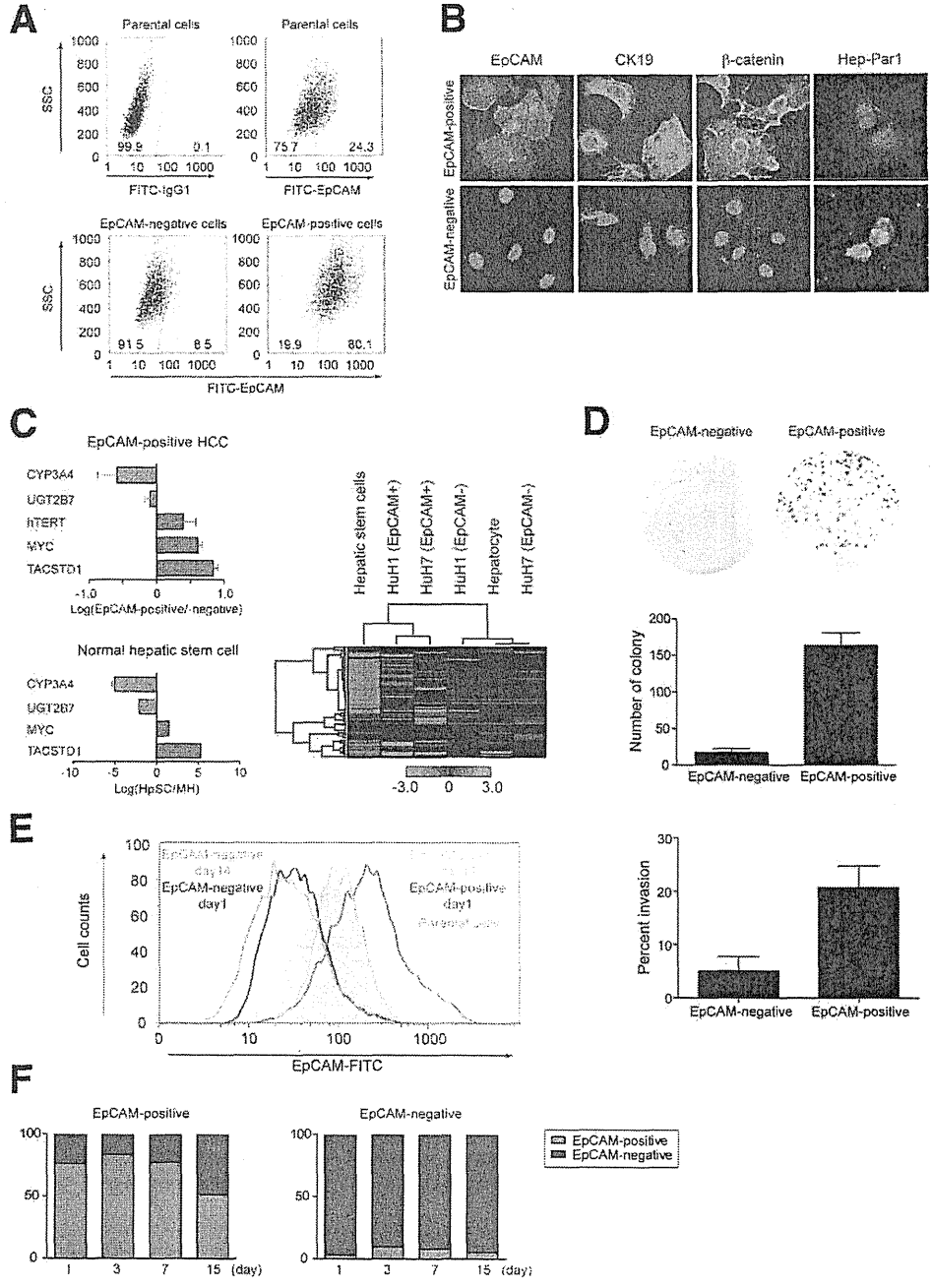

Figure 3. Characterization of EpCAM$^+$ and EpCAM$^-$ cells in HuH7 cells. (*A*) FACS analysis of EpCAM$^+$ and EpCAM$^-$ cells on day 1 after cell sorting. (*B*) IF analysis of cells stained with anti-EpCAM, anti-AFP, anti-CK19, or anti–β-catenin antibodies. (*C*) Quantitative reverse-transcription polymerase chain reaction analysis of EpCAM$^+$ and EpCAM$^-$ HuH7 cells (*left upper panel*) or HpSCs and MHs (*left lower panel*). Experiments were performed in triplicate. Hierarchical cluster analysis of HpSC, MH, and EpCAM$^+$ and EpCAM$^-$ HCC cells using a panel of genes expressed in human embryonic stem cells (*right panel*). Gene expression was measured in quadruplicate. (*D*) Representative photographs of the plates containing colonies derived from 2000 EpCAM$^+$ or EpCAM$^-$ HuH7 cells (*upper panel*). Colony formation experiments were performed in triplicate (mean ± SD) (*middle panel*). Cell invasiveness of EpCAM$^+$ and EpCAM$^-$ cells using the Matrigel invasion assay (*lower panel*). (*E*) Flow cytometer analysis of EpCAM$^+$ and EpCAM$^-$ HuH7 cells stained with anti-EpCAM at days 1 and 14 after cell sorting. (*F*) Percentage of sorted EpCAM$^+$ and EpCAM$^-$ cells after culturing for various times as analyzed by IF. Numbers of EpCAM$^+$ and EpCAM$^-$ cells were counted in 3 independent areas of chamber slides at days 1, 3, 7, and 15 after cell sorting. The average percentages of EpCAM$^+$ or EpCAM$^-$ cells are depicted as *red* or *blue*, respectively.

The isolated EpCAM$^+$ HuH7 cells formed colonies efficiently whereas EpCAM$^-$ cells failed to do so (Figure 3*D*, *upper* and *middle panels*; and Supplementary Figure 2*A* for HuH1 cells; see supplementary material online at www.gastrojournal.org). In addition, EpCAM$^+$ HuH7 cells were much more invasive than EpCAM$^-$ cells ($P <$ .03) (Figure 3*D*, *lower panel*; and Supplementary Figure 2*B* for HuH1 cells; see supplementary material online at www.gastrojournal.org). The EpCAM$^+$ fraction decreased with time in sorted EpCAM$^+$ HuH7 cells from greater than 80% to 50% (Figure 3*E*). However, a small percentage of EpCAM$^+$ cells remained constant in sorted EpCAM$^-$ HuH7 cells. FACS analysis confirmed the results of IF analysis (Figure 3*F* and Supplementary Figure 2*C* for HuH7 and HuH1 cells, respectively; see supplementary material online at www.gastrojournal.org), suggesting that EpCAM$^+$ cells could differentiate into EpCAM$^-$ cells, eventually allowing an enriched EpCAM$^+$ fraction to revert back to parental cells after 14 days of culture. In contrast, EpCAM$^-$ cells maintained their EpCAM$^-$ status. In addition, we successfully isolated 12 HuH1 and 2 HuH7 colonies from 192 single-cell–plated culture wells.

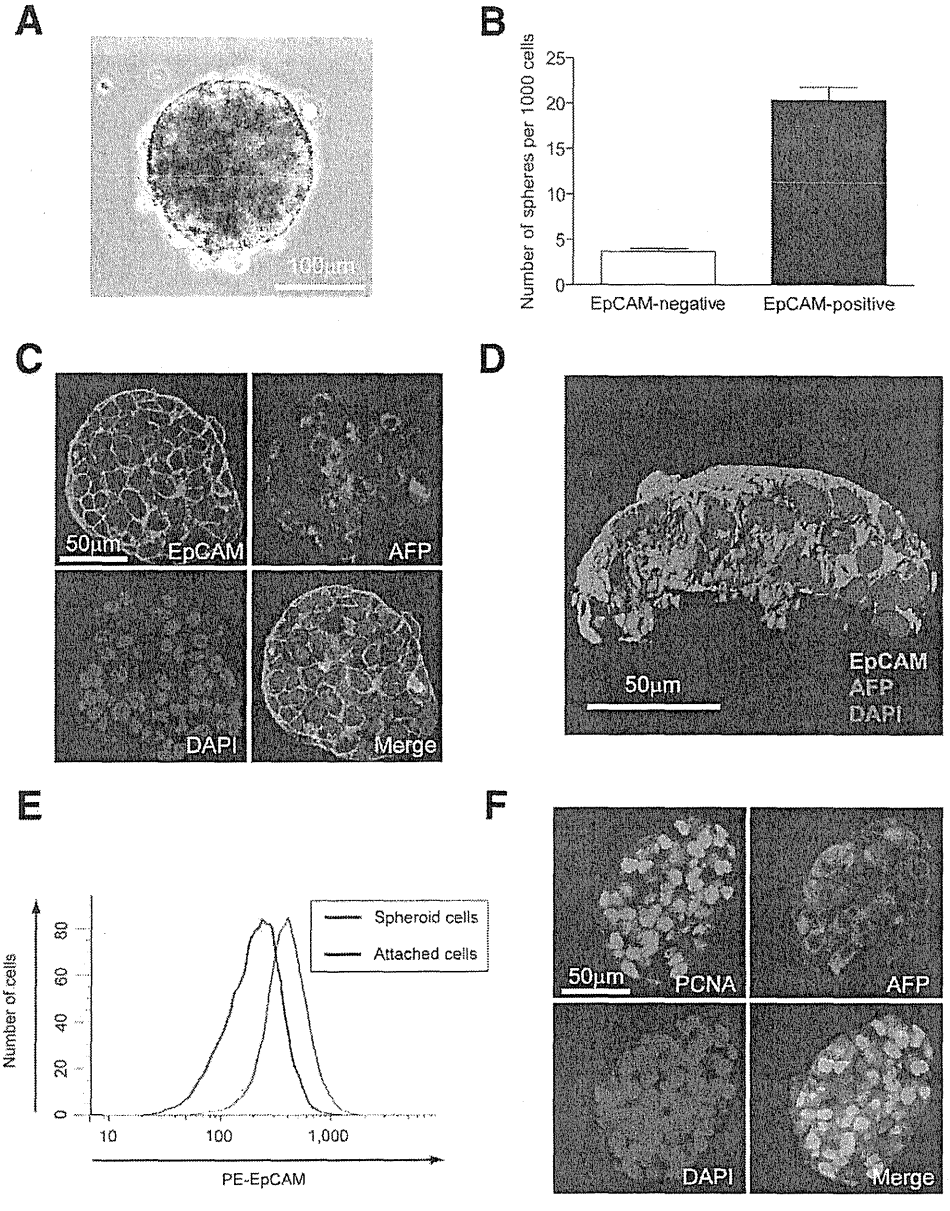

Figure 4. Spheroid formation of EpCAM$^+$ HuH1 HCC cells. (*A*) A representative phase-contrast image of an HCC spheroid derived from an EpCAM$^+$ cell (*scale bar*, 100 μm) and (*B*) total numbers of spheroids from 1000 sorted cells are shown. Experiments were performed in triplicate and data are shown as mean ± SD. (*C*) Representative confocal images of an HCC spheroid co-stained with anti-EpCAM, anti-AFP, and 4′,6-diamidino-2-phenylindole (DAPI) (*scale bar*, 50 μm). (*D*) A 3-dimensional image of an HCC spheroid co-stained with anti-EpCAM, anti-AFP, and DAPI (*scale bar*, 50 μm) reconstructed from confocal images using surface rendering. (*E*) FACS analysis of EpCAM$^+$ cells cultured as spheroid cells (*red*) or attached cells (*blue*) for 14 days after cell sorting. (*F*) Confocal images of an HCC spheroid co-stained with anti-PCNA, anti-AFP, and DAPI (*scale bar*, 50 μm).

However, all colonies were heterogeneous in EpCAM and AFP expression and no colony was completely EpCAM$^-$ (data not shown). Taken together, these results indicate that EpCAM$^+$ HCC cells resemble HpSC features. It appears that EpCAM$^+$ cells, but not EpCAM$^-$ cells, have self-renewal and differentiation capabilities with the ability to form colonies from a single cell, and produce both EpCAM$^+$ and EpCAM$^-$ cells.

It has been shown previously that stem/progenitor cells and cancer stem/progenitor cells can form spheroids in vitro in a nonattached condition.[36,37] Consistently, EpCAM$^+$ cells could form spheroids efficiently, reaching to about 150 to approximately 200 μm in diameter after 14 days of culture (Figure 4*A* and *B*). Interestingly, all cells in a spheroid were EpCAM$^+$, whereas AFP expression was relatively heterogeneous (Figure 4*C* and *D*, and Supplementary movie 1; see supplementary material online at www.gastrojournal.org). Rarely, a few spheroids derived from an EpCAM$^-$ cell fraction were positive for EpCAM (data not shown), suggesting that these spheroids were derived from contaminated residual EpCAM$^+$ cells by FACS sorting. All spheroid cells maintained EpCAM expression while half of the attached cells lost EpCAM expression when the EpCAM$^+$ fraction was cultured for 14 days (Figure 4*E*). Most spheroid cells also abundantly expressed proliferating cell nuclear antigen (PCNA), implying active cell proliferation (Figure 4*F* and Supplementary movie 2; see supplementary material online at www.gastrojournal.org). Thus, a subset of EpCAM$^+$ cells, but not EpCAM$^-$ cells, can form spheroids.

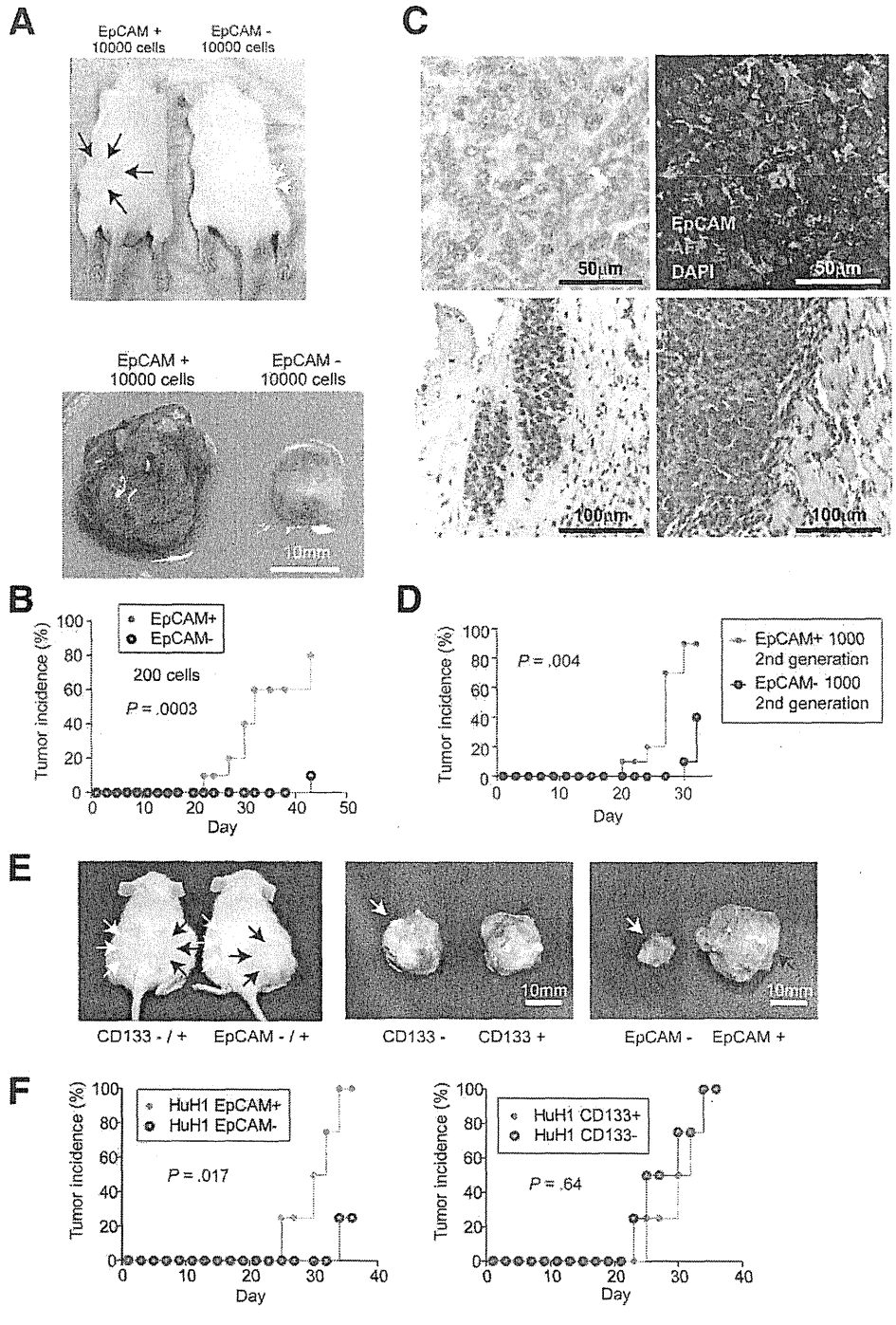

Figure 5. Tumorigenic and invasive potential of EpCAM$^+$ HCC cells. (*A*) Representative NOD/SCID mice (*upper panel*) with subcutaneous tumors (*lower panel*) from EpCAM$^+$ (*black arrows*) or EpCAM$^-$ (*white arrows*) HuH1 cells. (*B*) Tumorigenicity of 200 sorted HuH1 cells. (*C*) Histologic analysis of EpCAM$^+$ HuH1-derived xenografts. H&E staining of a subcutaneous tumor (*left upper panel*) with capsular invasion (*left lower panel*) and muscular invasion (*right lower panel*) and IF of the tumor stained with anti-EpCAM, anti-AFP, and 4′,6-diamidino-2-phenylindole (DAPI) (*right upper panel*) (*scale bar*, 50 μm). (*D*) Tumorigenicity of 1000 sorted cells derived from an EpCAM$^+$ HuH1 xenograft. Data are generated from 10 mice in each group. (*E*) Representative NOD/SCID mice (*left panel*) with subcutaneous tumors from CD133$^+$ (*black arrows*) or CD133$^-$ (*white arrows*) (*middle panel*) and EpCAM$^+$ (black arrows) or EpCAM$^-$ (*white arrows*) (*right panel*) HuH1 cells. (*F*) Tumorigenicity of 1000 HuH1 cells sorted by anti-EpCAM (*left panel*) or anti-CD133 (*right panel*) antibodies.

EpCAM$^+$ HCC Cells as Tumor-Initiating Cells

EpCAM$^+$ HCC cells, but not EpCAM$^-$ HCC cells, could efficiently initiate invasive tumors in NOD/SCID mice (Figure 5). For example, 10,000 EpCAM$^+$ HuH1 cells produced large hypervascular tumors in 100% of mice whereas EpCAM$^-$ cell fractions produced only small and pale-looking tumors in 30% of mice 4 weeks after injection (Figure 5*A* and Supplementary Figure 3*A*; see supplementary material online at www.gastrojournal.org). Similar results were obtained with HuH7 cells (Supplementary Figure 3*B–D*; see supplementary material online at www.gastrojournal.org). As little as 200 EpCAM$^+$ cells could initiate tumors in 8 of 10 injected mice, whereas 200 EpCAM$^-$ cells produced only 1 tumor among 10 injected mice at 6 weeks after transplantation, and the tumor sizes were much larger in the EpCAM$^+$ cells than in the EpCAM$^-$

cells (Figure 5*B* and Supplementary Figure 3*E*; see supplementary material online at www.gastrojournal.org). EpCAM$^+$ cells produced tumors with a mixture of both EpCAM$^+$ and EpCAM$^-$ cells in xenografts, and these cells invaded in the capsule and muscles of the leg adjacent to the tumor (Figure 5*C*). EpCAM$^+$ cells derived from tumors again maintained their tumor-initiating capacity, tumor morphology, and invasive ability in an in vivo serial transplantation experiment (Figure 5*D*). Occasionally, EpCAM$^-$ cell fractions produced a few small tumors that always contained a mixture of EpCAM$^+$ and EpCAM$^-$ cells (data not shown), indicating that the contaminated EpCAM$^+$ cells from FACS sorting contribute to the tumor-initiating ability.

To further validate whether EpCAM$^+$ HCC cells were tumor-initiating cells, we isolated EpCAM$^+$ HCC cells from 2 cases of AFP$^+$ (>600 ng/mL serum AFP) HCC clinical specimens using MACS. Consistently, 1×10^4 EpCAM$^+$ cells could induce tumors in NOD/SCID mice, but up to 1×10^6 EpCAM$^-$ cells failed to do so (Table 1). In addition, similar to HCC cell lines, fresh EpCAM$^+$ tumor cells from 2 clinical HCC specimens were more efficient in forming spheroids in vitro than EpCAM$^-$ cells (Supplementary Figure 4; see supplementary material online at www.gastrojournal.org).

FACS analysis results indicate that a majority of EpCAM$^+$ cells express CD133 in HuH7 cells but not in HuH1 cells (Figure 2*B*), which prompted us to compare the tumorigenic capacity of EpCAM$^+$ and CD133$^+$ cells in these cell lines. Noticeably, EpCAM$^+$ HuH1 cells showed marked tumor-initiating capacity compared with CD133$^+$ HuH1 cells (Figure 5*E* and *F*), whereas EpCAM$^+$ and CD133$^+$ cells had similar tumorigenic ability in HuH7 cells (data not shown).

GSK-3β Inhibition Augments EpCAM$^+$ HCC Cells

To determine the role of Wnt/β-catenin signaling[28] in EpCAM$^+$ HCC cells (Figure 1*B*), we first treated HuH1, HuH7, and HLF cells with a GSK-3β inhibitor BIO (Figure 6*A*), which activates Wnt/β-catenin signaling (Figure 6*B*) and maintains undifferentiation of embryonic stem cells.[38] 6-bromoindirubin-3′-oxime (BIO) increased the EpCAM$^+$ cell population in HuH1 and HuH7 cells when compared with the control methylated BIO (MeBIO) (Figure 6*A*). In contrast, BIO had no effect on the CD90$^+$ cell population, which is more tumorigenic than the CD90$^-$ cell population in HLF (Figure 6*A* and data not shown). Enrichment of EpCAM$^+$ cells was provoked further by the treatment of Wnt10B-conditioned media in HuH7 cells (Figure 6*C*).[34] BIO induced morphologic alteration of HuH7 cells because most cells became small and round when compared with MeBIO and suppressed EpCAM$^-$ AFP$^-$ cell populations (Figure 6*D*). Moreover, BIO induced *TACSTD1*, *MYC*, and *hTERT* expression and spheroid formation (Figure 6*E* and *F*).

Table 1. The Tumor-Initiating Capacity of EpCAM$^+$ Cells From Clinical HCC Specimens

HCC patients				Tumor incidence (mice with tumors/total no. of mice injected)	
No.	% of EpCAM$^+$ HCC cells	Groups	No. of cells injected	2 months	3 months
1	5.2	EpCAM$^+$	1×10^3	0/3	0/3
			1×10^4	2/3	2/3
			1×10^5	2/2	2/2
		EpCAM$^-$	1×10^5	0/3	0/3
			1×10^6	0/2	0/2
2	1.4	EpCAM$^+$	1×10^3	0/2	0/2
			1×10^4	0/1	1/1
		EpCAM$^-$	1×10^4	0/3	0/3
			1×10^5	0/2	0/2

EpCAM Blockage by RNA Interference

One of the hallmarks of CSCs is its resistance to conventional chemotherapeutic agents resulting in tumor relapse and thus targeting CSCs is critical to achieve successful tumor remission. Consistently, 5-FU could increase the EpCAM$^+$ population and spheroid formation of HuH1 and HuH7 cells (Figure 7*A* and *B*) (data not shown), suggesting a differential sensitivity of EpCAM$^+$ and EpCAM$^-$ HCC cells to 5-FU. In contrast, EpCAM blockage via RNA interference dramatically decreased the population of EpCAM$^+$ cells (Figure 7*C*), and significantly inhibited cellular invasion, spheroid formation, and tumorigenicity of HuH1 cells (Figure 7*D–F*). Thus, EpCAM may serve as a molecular target to eliminate HCC cells with stem/progenitor cell features.

Discussion

The cellular origin of HCC is currently in debate. In this study, we found that EpCAM can serve as a marker to enrich HCC cells with tumor-initiating ability and with some stem/progenitor cell traits. EpCAM is expressed in many human cancers with an epithelial origin.[39] During embryogenesis, EpCAM is expressed in fertilized oocytes, embryonic stem cells, and embryoid bodies, suggesting its role in early stage embryogenesis.[40] Furthermore, a recent article indicated that EpCAM is expressed in colonic and breast CSCs.[41] Taken together, these data suggest a critical role of EpCAM in CSCs as well as embryonic and somatic stem cells. Consistently, we found that EpCAM expression is regulated by Wnt/β-catenin signaling[29] and tumorigenic and highly invasive HpSC-HCC is orchestrated by a subset of cells expressing EpCAM and AFP with stem cell–like features and self-renewal and differentiation capabilities regulated by Wnt/β-catenin signaling (this study). Thus, EpCAM may be a common gene expressed in undifferentiated normal cells and HCCs with activated Wnt/β-catenin signaling. It may act as a downstream molecule

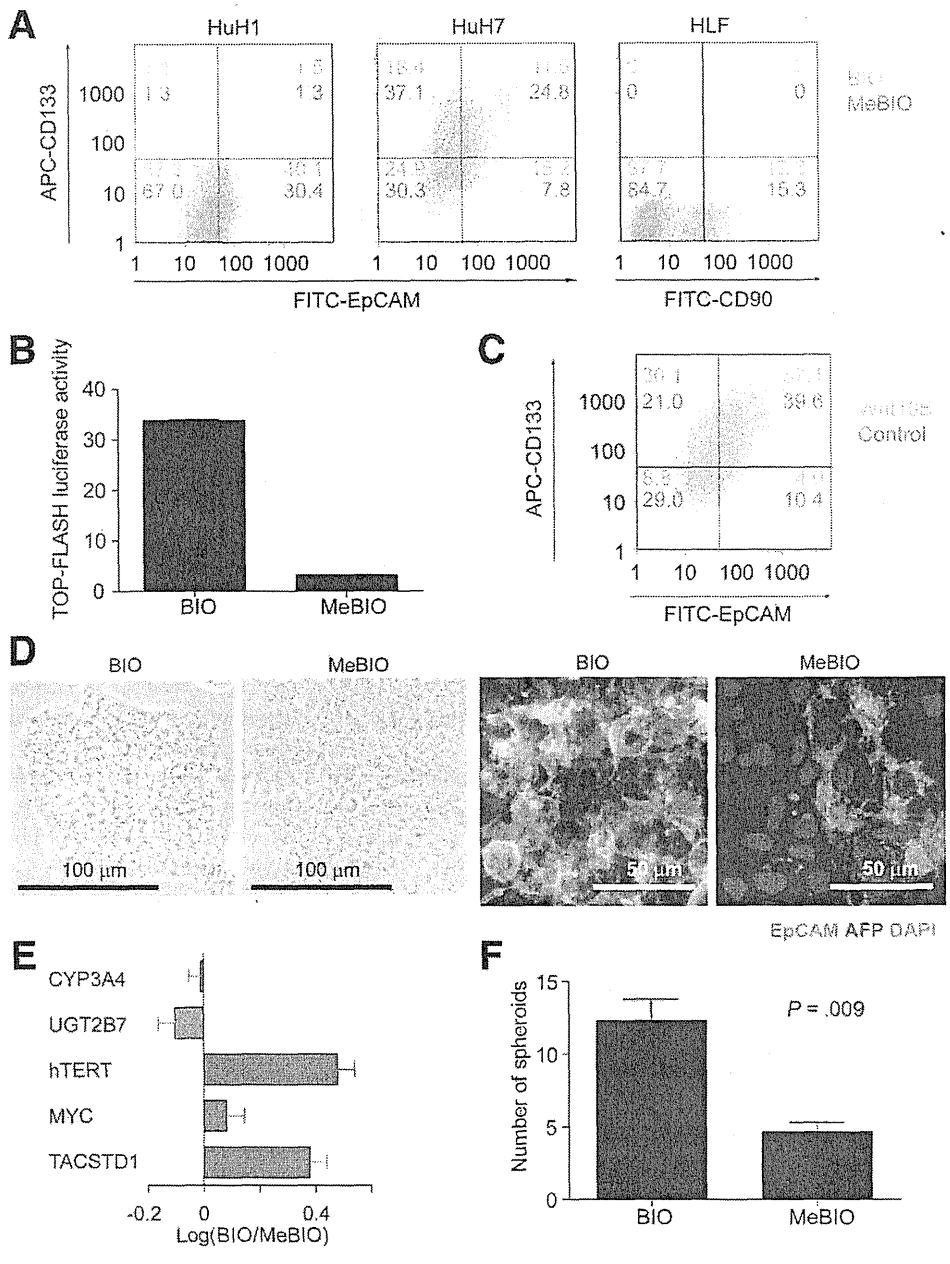

Figure 6. Wnt/β-catenin signaling augments EpCAM$^+$ HCC cells. (*A*) Flow cytometer analysis of HuH1, HuH7, and HLF cells treated with 2 μmol/L of BIO (*orange*) or MeBIO (*green*) for 10 days and stained with anti-EpCAM, anti-CD133 and anti-CD90 antibodies. (*B*) TOP-FLASH luciferase assays of HuH7 cells treated with 2 μmol/L of BIO or MeBIO. (*C*) Flow cytometer analysis of HuH7 cells cultured in normal media (Dulbecco's modified Eagle medium supplemented with 10% FBS) or Wnt10B conditioned media (details are described in the Materials and Methods section). Cells were cultured in each medium for 2 weeks. (*D*) Representative phase-contrast images (*left panel*: *scale bar*, 100 μm) or IF images (*right panel*: *scale bar*, 50 μm) of HuH7 cells treated with 2 μmol/L of BIO or MeBIO for 14 days. (*E*) Quantitative reverse transcription-polymerase chain reaction analysis of representative HpSC-HCC–related genes in HuH7 cells treated with 2 μmol/L of BIO or MeBIO for 14 days. (*F*) Spheroid formation assay of HuH7 cells treated with 2 μmol/L of BIO or MeBIO for 14 days (mean ± SD). FITC, fluorescein isothiocyanate.

to maintain HCC stemness and serve as a good marker for HCC initiating cells.

CD133 or CD90 have been used to identify potential hepatic CSCs.[35,42] CD133 is expressed in normal and malignant stem cells of the neural, hematopoietic, epithelial, hepatic, and endothelial lineages,[23,43,44] suggesting that CD133 is also a common marker to detect normal cells and CSCs. Captivatingly, EpCAM expression overlaps with CD133 expression in normal human colon tissues and colorectal cancer tissues, yet CD133$^+$ and CD133$^-$ cells are equally tumorigenic.[45] Similarly, we found that EpCAM$^+$ and EpCAM$^-$ HuH1 cells equally expressed CD133, but only EpCAM$^+$ cells developed large hypervascular tumors. Our data suggest that EpCAM may be a better marker than CD133 to enrich HCC tumor-initiating cells from AFP$^+$ tumors. We also found that CD90 expression was limited to HCC cell lines that are EpCAM$^-$ AFP$^-$, and Wnt/β-catenin signaling had little effect on CD90$^+$ cell enrichment. These results suggest that the expression patterns of various stem cell markers in tumor-initiating cells with stem/progenitor cell features may be different in each HCC subtype, possibly owing to the heterogeneity of activated signaling pathways in normal stem/progenitor cells where these tumor-initiating cells may originate. Therefore, it would be useful to

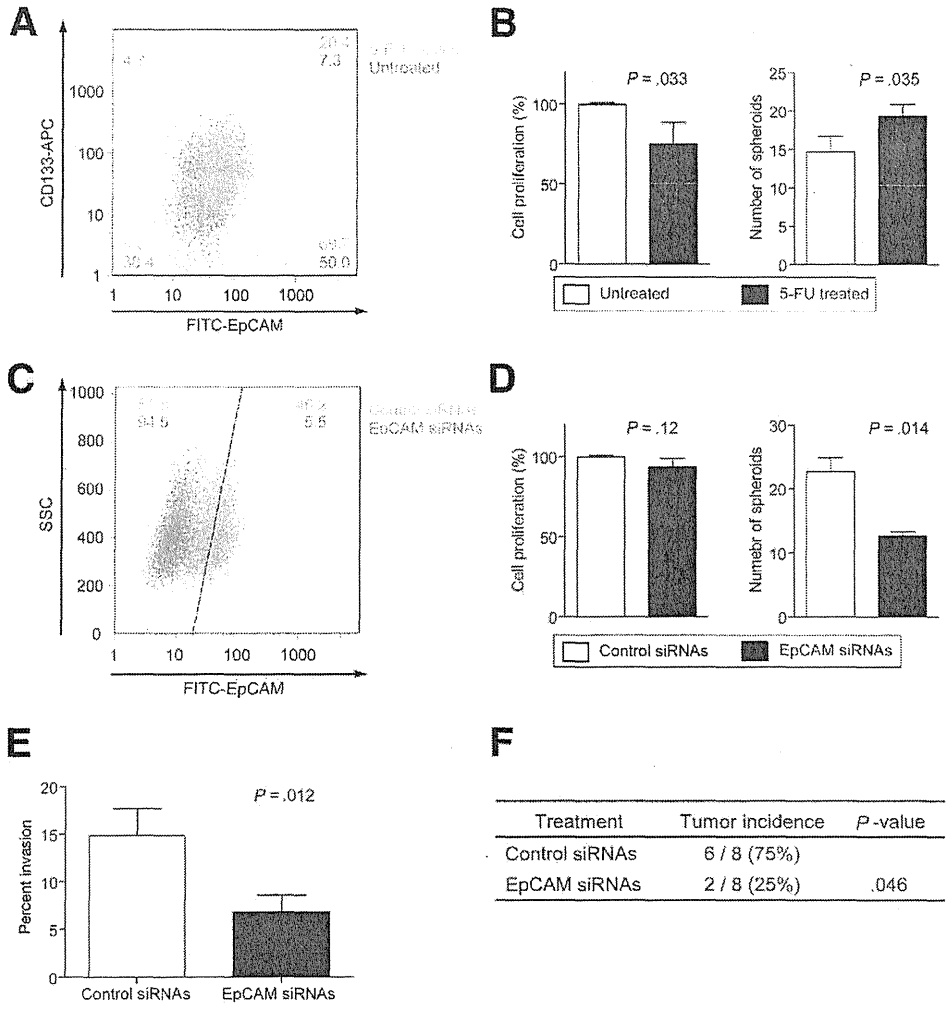

Treatment	Tumor incidence	*P*-value
Control siRNAs	6 / 8 (75%)	
EpCAM siRNAs	2 / 8 (25%)	.046

Figure 7. EpCAM blockage inhibits the tumorigenic and invasive capacity of EpCAM$^+$ HCC cells. (*A*) Enrichment of EpCAM$^+$ cells after 5-FU treatment. HuH1 cells refer as control or without treatment (*green*) or treated with 2 μg/mL of 5-FU (*orange*) for 3 days and analyzed by FACS using anti-EpCAM and anti-CD133 antibodies. (*B*) Spheroid formation of HuH1 cells treated with 2 μg/mL of 5-FU for 3 days. (*C*) FACS analysis of HuH1 cells treated with a control siRNA (orange) or EpCAM-specific siRNA (*green*) at day 3 after transfection. (*D*) Spheroid formation or (*E*) invasive capacity ofEpCAM$^+$ HuH1 cells transfected with a control siRNA or EpCAM-specific siRNA. Experiments were performed in triplicate and the data are shown as mean ± SD. (*D*) siRNAs. (*F*) Inhibition of tumor formation in vivo by EpCAM gene silencing. EpCAM$^+$ HuH1 cells were transfected with siRNA oligos and 1000 cells were injected 24 hours after transfection.

comprehensively investigate the expression patterns of stem cell markers to characterize the population of CSCs that may correlate with the activation of their distinct molecular pathways.

CSCs may be more resistant to chemotherapeutic agents than differentiated tumor cells possibly owing to an increased expression of adenosine triphosphate–binding cassette transporters and anti-apoptotic proteins.[4] Thus, the development of an effective strategy to target CSC pools together with conventional chemotherapies is essential to eradicate a tumor mass.[14] By blocking the programs that activate self-renewal and/or inhibit asymmetric division, CSC features could be destemmed.[46,47] Consistently, EpCAM blockage could inhibit cellular invasion and tumorigenicity of EpCAM$^+$ HCC cells, revealing the feasibility of targeting a CSC marker to destem CSC features. EpCAM may induce c-Myc,[48] a common molecular node activated in HpSC-HCC.[27] c-Myc, together with Oct3/4, Sox2, and Klf4, can induce pluripotent stem cells from adult fibroblasts.[49] It is possible that EpCAM blockage to inhibit hepatic CSCs may result in a suppression of c-Myc signaling. Encouragingly, EpCAM-specific antibodies are currently in phase II clinical trials.[50] Furthermore, a recent study indicated that EpCAM$^+$ circulating tumor cells identified by a unique microfluidic platform can be used to monitor outcomes of patients undergoing systemic treatment.[51] Therefore, it may be useful to combine EpCAM antibodies with conventional chemotherapy to target both CSCs and non-CSCs for the treatment of HCC.

Supplementary Data

Note: To access the supplementary material accompanying this article, visit the online version of *Gastroenterology* at www.gastrojournal.org, and at doi: 10.1053/j.gastro.2008.12.004.

References

1. Fialkow PJ. Clonal origin of human tumors. Biochim Biophys Acta 1976;458:283–321.

2. Heppner GH. Tumor heterogeneity. Cancer Res 1984;44:2259–2265.
3. Hanahan D, Weinberg RA. The hallmarks of cancer. Cell 2000; 100:57–70.
4. Jordan CT, Guzman ML, Noble M. Cancer stem cells. N Engl J Med 2006;355:1253–1261.
5. Clarke MF, Dick JE, Dirks PB, et al. Cancer stem cells—perspectives on current status and future directions: AACR Workshop on cancer stem cells. Cancer Res 2006;66:9339–9344.
6. Potter VR. Phenotypic diversity in experimental hepatomas: the concept of partially blocked ontogeny. The 10th Walter Hubert Lecture. Br J Cancer 1978;38:1–23.
7. Sell S. Cellular origin of cancer: dedifferentiation or stem cell maturation arrest? Environ Health Perspect 1993;101(Suppl 5): 15–26.
8. Wicha MS, Liu S, Dontu G. Cancer stem cells: an old idea—a paradigm shift. Cancer Res 2006;66:1883–1890.
9. Al Hajj M, Wicha MS, Benito-Hernandez A, et al. Prospective identification of tumorigenic breast cancer cells. Proc Natl Acad Sci U S A 2003;100:3983–3988.
10. Singh SK, Hawkins C, Clarke ID, et al. Identification of human brain tumour initiating cells. Nature 2004;432:396–401.
11. Bonnet D, Dick JE. Human acute myeloid leukemia is organized as a hierarchy that originates from a primitive hematopoietic cell. Nat Med 1997;3:730–737.
12. Ricci-Vitiani L, Lombardi DG, Pilozzi E, et al. Identification and expansion of human colon-cancer-initiating cells. Nature 2007; 445:111–115.
13. O'Brien CA, Pollett A, Gallinger S, et al. A human colon cancer cell capable of initiating tumour growth in immunodeficient mice. Nature 2007;445:106–110.
14. Dean M, Fojo T, Bates S. Tumour stem cells and drug resistance. Nat Rev Cancer 2005;5:275–284.
15. Rich JN. Cancer stem cells in radiation resistance. Cancer Res 2007;67:8980–8984.
16. Parkin DM, Bray F, Ferlay J, et al. Global cancer statistics, 2002. CA Cancer J Clin 2005;55:74–108.
17. Sell S, Pierce GB. Maturation arrest of stem cell differentiation is a common pathway for the cellular origin of teratocarcinomas and epithelial cancers. Lab Invest 1994;70:6–22.
18. Thorgeirsson SS, Grisham JW. Hepatic stem cells. Semin Liver Dis 2003;23:301.
19. Thorgeirsson SS, Grisham JW. Molecular pathogenesis of human hepatocellular carcinoma. Nat Genet 2002;31:339–346.
20. Lee JS, Heo J, Libbrecht L, et al. A novel prognostic subtype of human hepatocellular carcinoma derived from hepatic progenitor cells. Nat Med 2006;12:410–416.
21. Sigal SH, Brill S, Fiorino AS, et al. The liver as a stem cell and lineage system. Am J Physiol 1992;263:G139–G148.
22. Schmelzer E, Wauthier E, Reid LM. The phenotypes of pluripotent human hepatic progenitors. Stem Cells 2006;24:1852–1858.
23. Schmelzer E, Zhang L, Bruce A, et al. Human hepatic stem cells from fetal and postnatal donors. J Exp Med 2007;204:1973–1987.
24. Dan YY, Riehle KJ, Lazaro C, et al. Isolation of multipotent progenitor cells from human fetal liver capable of differentiating into liver and mesenchymal lineages. Proc Natl Acad Sci U S A 2006;103:9912–9917.
25. Zaret KS. Regulatory phases of early liver development: paradigms of organogenesis. Nat Rev Genet 2002;3:499–512.
26. Shafritz DA, Oertel M, Menthena A, et al. Liver stem cells and prospects for liver reconstitution by transplanted cells. Hepatology 2006;43:S89–S98.
27. Yamashita T, Forgues M, Wang W, et al. EpCAM and alpha-fetoprotein expression defines novel prognostic subtypes of hepatocellular carcinoma. Cancer Res 2008;68:1451–1461.
28. Reya T, Clevers H. Wnt signalling in stem cells and cancer. Nature 2005;434:843–850.
29. Yamashita T, Budhu A, Forgues M, et al. Activation of hepatic stem cell marker EpCAM by Wnt-β-catenin signaling in hepatocellular carcinoma. Cancer Res 2007;67:10831–10839.
30. Budhu A, Forgues M, Ye QH, et al. Prediction of venous metastases, recurrence and prognosis in hepatocellular carcinoma based on a unique immune response signature of the liver microenvironment. Cancer Cell 2006;10:99–111.
31. Ye QH, Qin LX, Forgues M, et al. Predicting hepatitis B virus-positive metastatic hepatocellular carcinomas using gene expression profiling and supervised machine learning. Nat Med 2003;9:416–423.
32. Wu CG, Forgues M, Siddique S, et al. SAGE transcript profiles of normal primary human hepatocytes expressing oncogenic hepatitis B virus X protein. FASEB J 2002;16:1665–1667.
33. Kubota H, Reid LM. Clonogenic hepatoblasts, common precursors for hepatocytic and biliary lineages, are lacking classical major histocompatibility complex class I antigen. Proc Natl Acad Sci U S A 2000;97:12132–12137.
34. Yoshikawa H, Matsubara K, Zhou X, et al. WNT10B functional dualism: beta-catenin/Tcf-dependent growth promotion or independent suppression with deregulated expression in cancer. Mol Biol Cell 2007;18:4292–4303.
35. Yang ZF, Ho DW, Ng MN, et al. Significance of CD90(+) cancer stem cells in human liver cancer. Cancer Cell 2008;13:153–166.
36. Dontu G, Abdallah WM, Foley JM, et al. In vitro propagation and transcriptional profiling of human mammary stem/progenitor cells. Genes Dev 2003;17:1253–1270.
37. Fang D, Nguyen TK, Leishear K, et al. A tumorigenic subpopulation with stem cell properties in melanomas. Cancer Res 2005; 65:9328–9337.
38. Sato N, Meijer L, Skaltsounis L, et al. Maintenance of pluripotency in human and mouse embryonic stem cells through activation of Wnt signaling by a pharmacological GSK-3-specific inhibitor. Nat Med 2004;10:55–63.
39. Balzar M, Winter MJ, de Boer CJ, et al. The biology of the 17-1A antigen (Ep-CAM). J Mol Med 1999;77:699–712.
40. Trzpis M, McLaughlin PM, de Leij LM, et al. Epithelial cell adhesion molecule: more than a carcinoma marker and adhesion molecule. Am J Pathol 2007;171:386–395.
41. Dalerba P, Dylla SJ, Park IK, et al. Phenotypic characterization of human colorectal cancer stem cells. Proc Natl Acad Sci U S A 2007;104:10158–10163.
42. Ma S, Chan KW, Hu L, et al. Identification and characterization of tumorigenic liver cancer stem/progenitor cells. Gastroenterology 2007;132:2542–2556.
43. Yin AH, Miraglia S, Zanjani ED, et al. AC133, a novel marker for human hematopoietic stem and progenitor cells. Blood 1997;90: 5002–5012.
44. Fargeas CA, Corbeil D, Huttner WB. AC133 antigen, CD133, prominin-1, prominin-2, etc.: prominin family gene products in need of a rational nomenclature. Stem Cells 2003;21:506–508.
45. Shmelkov SV, Butler JM, Hooper AT, et al. CD133 expression is not restricted to stem cells, and both CD133+ and CD133- metastatic colon cancer cells initiate tumors. J Clin Invest 2008; 118:2111–2120.
46. Hill RP, Perris R. "Destemming" cancer stem cells. J Natl Cancer Inst 2007;99:1435–1440.
47. Piccirillo SG, Reynolds BA, Zanetti N, et al. Bone morphogenetic proteins inhibit the tumorigenic potential of human brain tumour-initiating cells. Nature 2006;444:761–765.
48. Munz M, Kieu C, Mack B, et al. The carcinoma-associated antigen EpCAM upregulates c-myc and induces cell proliferation. Oncogene 2004;23:5748–5758.

49. Takahashi K, Tanabe K, Ohnuki M, et al. Induction of pluripotent stem cells from adult human fibroblasts by defined factors. Cell 2007;131:861–872.
50. Chaudry MA, Sales K, Ruf P, et al. EpCAM an immunotherapeutic target for gastrointestinal malignancy: current experience and future challenges. Br J Cancer 2007;96:1013–1019.
51. Nagrath S, Sequist LV, Maheswaran S, et al. Isolation of rare circulating tumour cells in cancer patients by microchip technology. Nature 2007;450:1235–1241.

Received March 9, 2008. Accepted December 1, 2008.

Reprint requests

Address requests for reprints to: Xin Wei Wang, PhD, Liver Carcinogenesis Section, Laboratory of Human Carcinogenesis, Center for Cancer Research, National Cancer Institute, 37 Convent Drive, Building 37, Room 3044A, MSC 4258, Bethesda, Maryland 20892-4258. e-mail: xw3u@nih.gov; fax: (301) 496-0497.

Acknowledgments

Microarray data are available publicly at http://www.ncbi.nlm.nih.gov/geo/ (accession number: GSE5975).

The authors thank Drs Curtis Harris and Sharon Pine for critical readings of the manuscript; Ms Barbara Taylor and Dr Susan Garfield for technical assistance; Drs Ali Brivanlou (Rockefeller University), Steve Strom (University of Pittsburgh), and Bert Vogelstein (Johns Hopkins University) for generously providing their research materials.

Conflicts of interest

The authors disclose no conflicts.

Funding

The authors disclose the following: This work was supported in part by the Intramural Research Program of the Center for Cancer Research, the US National Cancer Institute. Dr Yang, Dr HY Wang, Dr Jia, Dr Ye, Dr Qin, and Dr Tang were supported by research grants from the China National Natural Science Foundation for Distinguished Young Scholars (30325041) and the China National "863" R&D High-Tech Key Project (2002BA711A02-4). Dr Reid was supported by a sponsored research grant from Vesta Therapeutics (Research Triangle Park, NC), National Institutes of Health grants (R01 AA014243 and R01 IP30-DK065933), and a US Department of Energy grant (DE-FG02-02ER-63477). Sponsors had no role in the study design, data collection, analysis, and interpretation. Dr Yamashita, Dr Ji, Dr Budhu, Dr Forgues, Dr Yang, Dr Wang, Dr Jia, Dr Ye, Dr Wauthier, Dr Minato, Dr Honda, Dr Kaneko, and Dr Wang disclose no conflicts.

Supplementary Materials and Methods

FACS and MACS Analyses

Cultured cells were trypsinized, washed, and resuspended in Hank's balanced salt solutions (Lonza, Basel, Switzerland) supplemented with 1% HEPES and 2% fetal bovine serum. Cells then were incubated with FITC-conjugated anti-EpCAM monoclonal antibody Clone Ber-EP4 (DAKO, Carpinteria, CA) on ice for 30 minutes, and $EpCAM^+$ and $EpCAM^-$ cells were isolated by a BD FACSAria cell sorting system (BD Biosciences). For magnetic separation, cells were labeled 24 hours after enzymatic dissociation with primary EpCAM antibody (mouse IgG1; Dako), subsequently magnetically labeled with rat anti-mouse IgG1 Microbeads, and separated on a MACS LS column (Miltenyi Biotec, Inc, Auburn, CA). All the procedures were performed according to the manufacturer's instructions. The purity of sorted cells was evaluated by FACS. Fixed cells also were analyzed by FACS using a FACSCalibur (BD Biosciences). Anti-EpCAM antibody VU-1D9, anti-CD133/2 clone 293C3 (Miltenyi Biotec Inc), and anti-CD90 clone 5E10 (StemCell Technologies Inc, Vancouver, British Columbia, Canada) were used to detect $EpCAM^+$, $CD133^+$, or $CD90^+$ cells. Intracellular AFP levels were examined by a BD Cytofix/Cytoperm Fixation/Permeabilization Kit (San Jose, CA) and anti-AFP rabbit polyclonal antibody (DAKO).

Quantitative Reverse Transcription–Polymerase Chain Reaction and IHC Analyses

Total RNA was extracted using TRIzol (Invitrogen) according to the manufacturer's instructions. The expression of selected genes was determined in triplicate using the Applied Biosystems 7500 Sequence Detection System (Applied Biosystems, Foster City, CA) as previously described.[1] Genes expressed in embryonic stem cells were determined in quadruplicate using TaqMan Human Stem Cell Pluripotency Array (Applied Biosystems). IHC analyses with specific antibodies were performed essentially as previously described.[1] Confocal fluorescence microscopic analysis was performed essentially as previously described.[2]

References

1. Yamashita T, Forgues M, Wang W, et al. EpCAM and alpha-fetoprotein expression defines novel prognostic subtypes of hepatocellular carcinoma. Cancer Res 2008;68:1451–1461.
2. Wang W, Budhu A, Forgues M, et al. Temporal and spatial control of nucleophosmin by the Ran-Crm1 complex in centrosome duplication. Nat Cell Biol 2005;7:823–830.

Supplemetary Table 1. Clinicopathologic Characteristics of HpSC-HCC and MH-HCC Cases Used for Oligonucleotide Microarray Analyses

Parameters	HpSC-HCC (n = 60)	MH-HCC (n = 96)	*P* value[a]
Mean age, *y* (SD)	46.0 ± 10.7	52.9 ± 10.5	.0004
Sex: male/female	50/10	87/9	.18
Cirrhosis: yes/no/no data	56/4	88/7/1	.72
Median AFP level, *ng/mL* (25%–75%)	1706 (865–5915)	11.8 (4.0–48.6)	<.0001
Histologic grade[b]			
I–II	14	41	
II–III	44	48	
III–IV	2	5	
No data	0	2	.031
Mean tumor size, *cm* (SD)	5.1 ± 3.0	4.4 ± 3.0	.088
Multinodular: yes/no	16/44	15/81	.09
Portal vein invasion, yes/no[c]	11/49	9/87	.10
TNM classification			
I	24	46	
II	22	42	
III	14	8	.03
Virus status: HBV/HBV + HCV/unknown	56/4/0	95/0/1	.43

[a]Mann–Whitney *U* test or χ^2 test.
[b]Edmondson–Steiner.
[c]Macroscopic portal vein invasion.

Supplementary Table 2. Clinicopathologic Characteristics of HpSC-HCC and MH-HCC Cases Used for IHC

Parameters	HpSC-HCC (*n* = 24)	MH-HCC (*n* = 55)	*P* value[a]
Mean age, *y* (SD)	46.4 ± 9.4	58.4 ± 11.9	< .0001
Sex: male/female	20/4	48/7	.64
Cirrhosis: yes/no	23/1	46/9	.14
Median AFP level, *ng/mL* (25%–75%)	1620 (887–3166)	12 (9.3–219)	< .0001
Histologic grade[b]			
I–II	12	32	
II–III	8	21	
III–IV	4	2	.13
Mean tumor size, *cm* (SD)	7.1 ± 3.6	5.2 ± 3.6	.014
Multinodular: yes/no	4/20	16/39	.24
Portal vein invasion: yes/no[c]	12/12	12/43	.012
TNM classification			
I	4	19	
II	8	20	
III	12	16	.14
Virus status: HBV/HCV/unknown	21/2/1	32/21/2	.026

[a]Mann–Whitney *U* test or χ^2 test.
[b]Edmondson–Steiner.
[c]Macroscopic portal vein invasion.

Supplementary Table 3. Top 10 List of Canonical Pathways Activated in HpSC-HCC From Ingenuity Pathway Analysis

Pathways	Genes included in cluster A
Axonal guidance signaling	
Up	ROBO2, ARPC5L (includes EG:81873), SEMA4G, PDGFRB, PLCB1, PRKCD, FGFR3, FZD5, MERTK, DDR1, LINGO1, SEMA3C
Down	PIK3C3, IGF1, PIK3C2G, MAP2K2, ARHGEF15
Transforming growth factor-β signaling	
Up	PDGFRB, FGFR3, MERTK, UBD, DDR1, SMAD5
Down	MAP2K2, HNF4A
Integrin signaling	
Up	ARPC5L (includes EG:81873), PDGFRB, FGFR3, GRB7, MERTK, ITGB5, DDR1, DDEF1
Down	PIK3C3, MYLK, PIK3C2G, MAP2K2
Apoptosis signaling	
Up	PDGFRB, BAK1, CYCS, FGFR3, MERTK, DDR1
Down	MAP3K5, MAP2K2
G2/M DNA damage checkpoint regulation	
Up	YWHAZ, CCNB2, UBD, WEE1
Down	CDKN2A, GADD45A
ERK/MAPK signaling	
Up	ELF3, PDGFRB, YWHAZ, PRKCD, FGFR3, MERTK, DDR1
Down	PIK3C3, DUSP1, PIK3C2G, ESR1, MAP2K2
Wnt/β-catenin signaling	
Up	DKK1, SOX9, FZD5, UBD, TCF7L2, CSNK1E
Down	CDKN2A, RARG
PI3K/AKT signaling	
Up	PDGFRB, YWHAZ, FGFR3, MERTK, DDR1
Down	MAP3K5, MAP2K2, GYS2
Amyloid processing	
Up	BACE2, CSNK1E, MAPK13
Down	
Leukocyte extravasation signaling	
Up	PRKCD, CLDN4, CLDN1, MMP11, MAPK13
Down	PIK3C3, CLDN2, PIK3C2G, MAP2K2

NOTE. The top 10 pathways were selected based on the significance for the enrichment of the genes with a particular canonical signaling pathway determined by the one-sided Fisher exact test ($P < .01$).

Supplementary Table 4. Top 10 List of Canonical Pathways Activated in MH-HCC From Ingenuity Pathway Analysis

Pathways	Genes included in cluster B
Lipopolysaccharide/interleukin-1–mediated inhibition of RXR function	
Up	SULT1C2, ACSL4, ACSL3, FABP5, GSTP1
Down	NR1I2, NR1I3, CYP7A1, ALDH1L1, ABCB1, SLC10A1, SLC27A2, CD14, GSTM1, ALDH6A1, GSTM4, ACSL5, CES2 (includes EG:8824), FMO3, SULT2A1 (includes EG:6822), GSTA1, CYP2C8, LC27A5, CYP3A7, ABCG5, ALDH8A1, APOC4 (includes EG:346), CYP3A4, ACSL1, ABCB11, FMO4, MAOA
Xenobiotic metabolism signaling	
Up	SULT1C2, PRKCD, GSTP1, MAPK13
Down	NR1I2, NR1I3, ALDH1L1, ABCB1, UGT2B15, MAP2K2, UGT2B7, PPARGC1A, GSTM1, PIK3C3, ALDH6A1, GSTM4, CES2 (includes EG:8824), MAP3K5, FMO3, PIK3C2G, SULT2A1 (includesEG:6822), CYP1A2, GSTA1, CYP2C8, CYP3A7, NQO2, ALDH8A1, CYP3A4, CES1 (includes EG:1066), FMO4, MAOA
Hepatic cholestasis	
Up	ADCY3, PRKCD
Down	CD14, ABCG5, NR1I2, CYP7A1, CYP7B, CYP8B1, ABCB1, ESR1, SLC10A1, ABCB11, ABCB4, HNF4A
Aryl hydrocarbon receptor signaling	
Up	GSTP1
Down	CDKN2A, NQO2, GSTM1, ALDH8A1, ALDH6A1, ALDH1L1, GSTM4, ESR1, CYP1A2, GSTA1, RARG
NRF2-mediated oxidative stress response	
Up	DNAJA4, PRKCD, GSTP1
Down	NQO2, GSTM1, AOX1, PIK3C3, GSTM4, MAP3K5, SOD1, PIK3C2G, MAP2K2, FKBP5, GSTA1
Complement system	
Up	
Down	C8A, C1R, MASP1, C6, C8B, MASP2
Coagulation system	
Up	
Down	SERPINC1, KLKB1, F9, KNG1 (includes EG:3827), F11
Acute-phase response signaling	
Up	MAPK13
Down	APCS, RBP5, C1R, MAP3K5, HRG, MAP2K2, KLKB1, SAA4
p53 signaling	
Up	THBS1
Down	CDKN2A, PIK3C3, SNAI2, GADD45A, PIK3C2G, GADD45B
LXR/RXR activation	
Up	HMGCR
Down	CD14, ABCG5, APOA5, CYP7A1, APOC4 (includes EG:346)

LXR/RXR, liver X receptor/retinoid X receptor; NRF2, NF-E2-related factor 2.
NOTE. The top 10 pathways were selected based on the significance for the enrichment of the genes with a particular canonical signaling pathway determined by the one-sided Fisher exact test ($P < .01$).

doi:10.1111/j.1440-1746.2008.05496.x

HEPATOLOGY

Rapid hepatic fate specification of adipose-derived stem cells and their therapeutic potential for liver failure

Agnieszka Banas,* Takumi Teratani,* Yusuke Yamamoto,*,† Makoto Tokuhara,‡ Fumitaka Takeshita,* Mitsuhiko Osaki,* Takashi Kato,† Hitoshi Okochi‡ and Takahiro Ochiya*

*Section for Studies on Metastasis, National Cancer Center Research Institute, Chuo-ku, †Department of Biology, School of Education, Waseda University, Shinjuku-ku, and ‡Department of Surgery, International Medical Center of Japan, Shinjuku, Tokyo, Japan

Key words
adipose, differentiation, hepatocyte, liver regeneration, mesenchymal stem cell.

Accepted for publication 13 April 2008.

Correspondence
Dr Takahiro Ochiya, Section for Studies on Metastasis, National Cancer Center Research Institute, 1-1, Tsukiji 5-chome, Chuo-ku, Tokyo 104-0045, Japan. Email: tochiya@ncc.go.jp

Abstract

Background and Aim: Multipotential mesenchymal stem cells (MSC), present in many organs and tissues, represent an attractive tool for the establishment of a successful stem cell-based therapy in the field of regeneration medicine. Adipose tissue mesenchymal stem cells (AT-MSC), known as adipose-derived stem cells (ASC) are especially attractive in the context of future clinical applications because of their high accessibility and minimal invasiveness during the procedure to obtain them. The goal of the present study was to induce human ASC into functional hepatocytes *in vitro* within a very short period of time and to check their therapeutic potential *in vivo*.

Methods: *In vitro* generated ASC-derived hepatocytes were checked for hepatocyte-specific markers and functions. Afterwards, they were transplanted into nude mice with liver injury. Twenty-four hours after transplantation, biochemical parameters were evaluated in blood serum.

Results: We have shown here that ASC can be differentiated into hepatocytes within 13 days and can reach the functional properties of primary human hepatocytes. After transplantation into mice with acute liver failure, ASC-derived hepatocytes can restore such liver functions as ammonia and purine metabolism. Markers of liver injury, alanine aminotransferase, aspartate aminotransferase, as well as ammonia, were decreased after ASC-derived hepatocyte transplantation.

Conclusions: Our data highlight the properties of ASC as having a special affinity for hepatocyte differentiation *in vitro* and liver regeneration *in vivo*. Thus, ASC may be a superior choice for the establishment of a therapy for injured liver.

Introduction

The liver is exposed to many factors such as drugs, xenobiotics and viruses, which cause chronic hepatitis and liver cirrhosis. In most cases these lead to hepatocellular carcinoma and finally to organ failure, where there is chronic inflammation, fibrosis and no longer any regeneration ability.[1]

At present, liver transplantation is the only effective treatment for severe liver injuries. However, because of organ rejection and lack of donors, alternative strategies are urgently needed.

Human primary hepatocytes are commercially available; however, maintaining them in *in vitro* culture is very difficult, if not nearly impossible. After a few days of *in vitro* culturing they lose their functions. Additionally, their usage does not solve the problem of rejection. These factors limit their experimental applications and exclude their clinical usage.

In the last few years, extrahepatic cell populations with the potential to impact liver diseases have been discovered. The potential candidate stem cells for therapy of an injured liver are mesenchymal stem cells (MSC), which can be obtained from different sources such as bone marrow (BM),[2] umbilical cord blood (UCB),[3] amniotic fluid (AF),[4] scalp tissue,[5] placenta,[6] or adipose tissue (AT)[7,8] of the human body. These cells reveal a multipotentiality and semi-infinite proliferation ability. The hepatogenic differentiation capacity of MSC has been confirmed in many independent studies on BM-MSC,[9–14] UCB-MSC,[15–16] and adipose-derived stem cells (ASC).[17–19] The possibility for their future application in the therapy of liver diseases is very promising. MSC can easily be obtained from a patient's own tissues, isolated *ex vivo*, expanded, differentiated toward hepatocytes, and transplanted back into the patient in the form of either undifferentiated MSC or MSC-derived hepatocytes. Such a possibility sidesteps the limits regarding ethical issues and immunocompatibility problems. Importantly, MSC represent an advantageous cell type for allogenic transplantation as well, because they are immuno-privileged with low major histocompatibility complex (MHC) I (histocompatibility

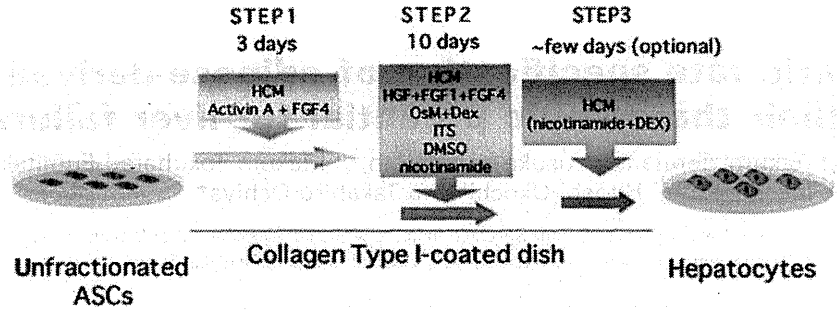

Figure 1 Improved and modified hepatogenic induction strategy. At present, approximately 2 weeks are required to induce hepatogenic characteristics in adipose-derived stem cells (ASC). Unfractionated ASC were plated on collagen type I-coated dishes and were treated with Activin A and FGF4 at step 1, followed by step 2, treatment with hepatocyte growth factor (HGF), fibroblast growth factor (FGF)1, FGF4, oncostatin M (OsM), dexamethasone, insulin-transferrin-selenium (ITS), dimethyl sulfoxide (DMSO), and nicotinamide. At this point, cells may be maintained a few days in hepatocyte culture medium (HCM) alone (or optionally supplemented with 10^{-8} mol/L dexamethasone and 0.05 mmol/L nicotinamide). MSC, mesenchymal stem cells.

lymphocyte antigen [HLA I]) and no MHC II (HLA II) expression, therefore reducing the risk of allogenic transplant rejection.[20–27]

Currently, attention is being given to adipose tissue (AT) as a source of MSC for regenerative medicine. From adipose tissue, a sufficient number of stem cells for a stem cell-based therapy may be obtained without invasiveness or damage to a patient's health. We have already demonstrated that human ASC have the ability to give rise to hepatocyte-like cells and that CD105 is a candidate mesenchymal stem cell marker.[19] However, this *in vitro* differentiation method is not applicable to a practical, clinical use, as more than 1 month is required to induce ASC into cells with hepatic functions.

In the present study, we evaluate the therapeutic potential of ASC-derived hepatocyte-like cells after transplantation into mice with liver injury. Clinical applications in the future would require a special approach, such as shortening as much as possible *ex vivo* manipulations, including cultivation and direct hepatic fate. Therefore, we improved and modified our hepatocyte differentiation strategy, based on the current knowledge on *in vivo* mouse fetal liver development. At present, a period as short as 13 days is required and that strategy is enriched by pretreatment with Activin A (PeproTech, EC, London, UK) and fibroblast growth factor (FGF)4 (PeproTech) (one of the factors secreted by septum transversum mesenchyme (STM) and cardiogenic mesoderm at the early stage of endoderm development *in vivo*). Additionally, we reorganized the content of the growth factor cocktail and enriched it with the addition of dimethyl sulfoxide (DMSO), nicotinamide and insulin-transferrin-selenium. Using the present protocol, we obtained functional hepatocyte-like cells in a much shorter period of time. Finally, we transplanted ASC-derived hepatocyte-like cells into immunodeficient mice with liver injury/non-severe acute liver injury. Our results showed a significant decrease of ammonia, aspartate aminotransferase (AST), alanine aminotransferase (ALT), and uric acid (UA) in the blood plasma of mice after ASC-derived hepatocyte-like cell transplantation. The results show a very important step towards future establishment of an alternative and successful therapy for liver disease.

Methods

Isolation and culturing of ASC

Adipose-derived stem cells were derived from abdominal subcutaneous adipose tissue, which was obtained from two female gastric cancer patients (Donor #1 [36 years old] and Donor #2 [45 years old]), undergoing gastrectomy at the International Medical Center of Japan, Tokyo. The hospital's committee of ethics approved this study, and informed consent was obtained from both patients. Adipose tissue was processed as previously described.[19] For *in vitro* differentiation, the cells (ASC062801, ASC012202, ASC0025) obtained from DS Pharma Biomedical Co., Osaka, Japan) were also analyzed.

Hepatic differentiation

At passage five to 10, the cells were plated on collagen type I-coated dishes at a concentration of $3.0–4.0 \times 10^4$ cells/cm^2 (Fig. 1). When the cells reached confluency, hepatogenic induction was carried out over a period of 2 weeks. First, the cells were treated for 3 days with DMEM (GibcoBRL, Tokyo, Japan) (serum free) supplemented with 20 ng/mL Activin A and 20 ng/mL FGF4 (PeproTech EC, London, UK). Afterwards, the cells were cultured for 10 days in a hepatocyte culture medium (HCM), containing 5 μg/mL transferrin, 10^{-6} mol/L hydrocortisone-21-hemisuccinate, 0.5 mg/mL bovine serum albumin, 2 mmol/L ascorbic acid, 20 ng/mL epidermal growth factor, 5 μg/mL insulin, 50 μg/mL gentamicin (Cambrex Corp., Walkersville, MD, USA) and supplemented with 150 ng/mL hepatocyte growth factor (HGF), 100 ng/mL FGF1, 25 ng/mL FGF4, 30 ng/mL oncostatin M (OsM; PeproTech), (2×10^{-5} mol/L) dexamethasone (Dex; Sigma, Tokyo, Japan), 1 × insulin-transferrin-selenium (ITS; Gibco), 0.05 mmol/L nicotinamide (Sigma), and 0.1% DMSO (Sigma). For the next few days, the cells were maintained with HCM alone. For *in vivo* transplantation, hepatocyte-like cells from two donors (#1 and #2) were harvested by treatment with a 0.05% collagenase/1000 U/mL dispase solution for 3–5 min, dissolved in

PBS (–) and injected intravenously into mice with liver injury caused by CCl_4 injection.

Quantitative real-time PCR

In order to confirm the regulation of the hepatocyte-specific genes in ASC-derived hepatocytes, we performed real-time polymerase chain reaction (PCR) for albumin (ALB) and tryptophan 2,3-dioxygenase (TDO2), with glyceraldehyde-3-phosphate dehydrogenase (GAPDH) as a reference gene. After retro-transcription, cDNA was subjected to real-time PCR by using Platinum Quantitative PCR Super Mix-UDG (Invitrogen, Tokyo, Japan) and specific primers for ALB (NM_000477): F:GTCACCAAATG CTGCACAGA, R:ACGAGCTCAACAAGTGCAGT for TDO2 (NM_005651): F:GTGTGCATGGTGCACAGAAT, R:GGGTT CATCTTCGGTATCCA, for FOXA2 (NM_021784): F:GGGA GCGGTGAAGATGGAAG, R:TGCCAGCGCCCACGTA and for GAPDH (NG_007073): F:GAAGGTGAAGGTCGGAGT, and R:GAAGATGGTGATGGGATTTC, based on the human genome database. The PCR conditions were as follows: denaturation at 95°C for 30 s, annealing at 56°C or 60°C for 30 s, and extension at 72°C for 30 s for up to 45 cycles. Real-time PCR was carried out by using the Applied Biosystems (Tokyo, Japan) PRISM 7700 Sequence Detection System.

Immunofluorescence

Cells were fixed in 4% formaldehyde for 10 min, followed by incubation with Protein Block (DakoCytomation, Carpinteria, CA, USA) for 30 min. ASC-derived hepatocytes were analyzed by immunohistochemistry using monoclonal anti-human specific albumin ALB (clone HAS-11, 1:250; Sigma) antibody overnight at 4°C. The Alexa Fluor 488 (green, 1:1000)-conjugated secondary antibody (Invitrogen, Tokyo, Japan) was applied for 30 min. Nuclei staining was performed using 4,6-diamidino-2-phenylindole (DAPI; Vector Laboratories, Burlingame, CA, USA).

Albumin production

Albumin production was evaluated by enzyme linked immunosorbent assay (ELISA, E80-129; Bethyl Laboratories, Montgomery, TX, USA). The antibody is human specific and does not cross-react with mouse, rat, bovine, goat, and pig albumin. Briefly, the supernatant during hepatogenic induction was collected every 3 days at days 3, 6 and 9, and ELISA assay was performed. Data are reported as the mean ± SD and were analyzed by Student's *t*-test, $n = 3$ ($^*P < 0.05$).

ASC-derived hepatocyte transplantation into mice with CCl_4-induced injury

Animal studies were carried out in compliance with the guidelines of the Institute for Laboratory Animal Research, National Cancer Center Research Institute. Six-week-old female BALB/c nude mice (CLEA Japan Inc., Tokyo, Japan) were used. An acute liver failure model was produced by giving one dose of CCl_4. At day 0, mice underwent i.p. injection of 100 μL/20 g bodyweight of olive oil containing 10 μL CCl_4. At day 1, mice underwent transplantation of ASC-derived hepatocyte-like cells (Donor #1 ($n = 4$), or Donor #2 ($n = 4$) at a concentration of 1.5×10^6 cells per mouse (0.2 mL cell suspension was injected through the tail vein). As a control, non-transplanted CCl_4-treated mice ($n = 3$) and non-transplanted CCl_4-non-treated (olive oil) ($n = 3$) mice were used. Twenty-four hours after transplantation, blood serum was collected and evaluated for biochemical parameters, such as AST, ALT, UA and ammonia concentration levels.

Assessment of liver functions

Blood samples were obtained from each mouse, centrifuged for 20 min at 400 *g* and serum was collected. Serum samples were tested for ammonia concentration level by using the Ammonia Test-Wako (Wako Pure Chemicals, Tokyo, Japan). The concentration of markers of liver injury such as ALT, AST and UA was analyzed by using a FUJIFILM DRI-CHEM 3500 machine and FUJI DRI-CHEM Slides for ALT/ALT-PIII, AST/AST-PIII, and UA-PIII, respectively (Fujifilm Co., Tokyo, Japan).

Statistical analysis

The results are given as the mean ± SD. Statistical analyses were conducted using either the variance with the Bonferroni correction for multiple comparisons or the Student's *t*-test. The statistical analysis of quantitative relative expression was evaluated by using the Pair Wise Fixed Reallocation Randomization Test©, Relative Expression Software Tool-XL = REST-XL© (http://www.gene-quantification.info/). A P value < 0.05 was considered significant.

Results

Hepatic fate specification of ASC

A direct fate hepatic specification (Fig. 1) was performed within 13 days. After that, ASC-derived hepatocyte-like cells could be maintained for a few days in HCM alone (optionally supplemented with Dex 10^{-8} mol/L and nicotinamide 0.05 mmol/L). After 3 days of pretreatment with FGF4 and Activin A, ASC expressed FOXA2 (Fig. 2a), the expression of which was decreased at day 6 of the induction system (3 days of pretreatment with FGF4 and Activin A, followed by 3 days of treatment with a cocktail containing HGF, FGF1, FGF4, OsM, Dex, ITS, DMSO and nicotinamide) (Fig. 2a). FOXA2, so-called hepatocyte nuclear factor 3β (HNF-3β) is an essential transcription factor for endoderm specification as well as hepatogenic fate. Similarly, ALB (hepatocyte-specific protein) and TDO2 (hepatocyte-specific enzyme, expressed by mature hepatocytes) were also detected by quantitative PCR at day 3 and their expression increased at day 6 of the induction system (Fig. 2a). The representative morphology of the ASC-derived hepatocyte-like cells of either a cancer patient's ASC or from the commercialized cells at the 13th day of induction is shown in Figure 2b. Importantly, 24 h of incubation with our new cocktail (Step II) alone is enough to dramatically influence the morphology of ASC (Donor #2) from fibroblast to epithelial (Fig. 3a). The pretreatment with Activin A and FGF4, however, is very important, because it induces the endodermal fate and alters further morphological changes and maturation of hepatocyte-like cells. As shown

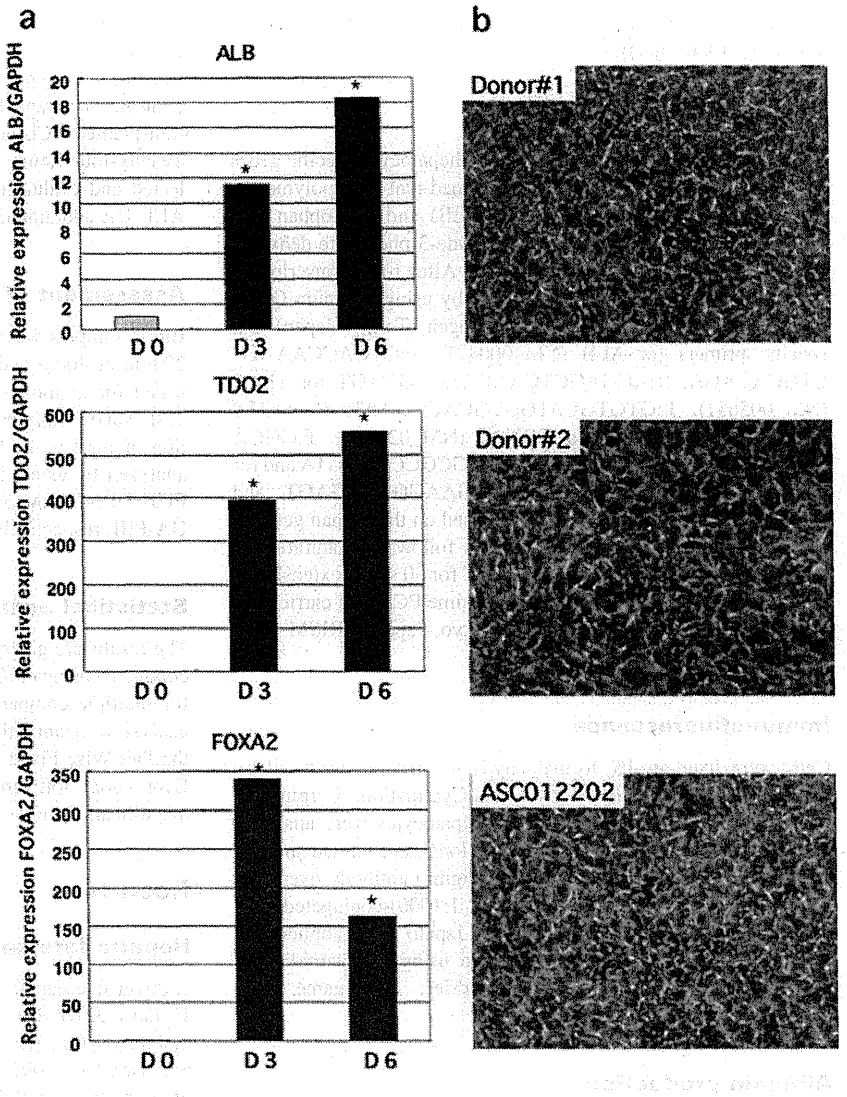

Figure 2 (a) Expression of albumin (ALB), tryptophan 2,3-dioxygenase (TDO2) and FOXA2 at day 3 (D3) (pretreatment with fibroblast growth factor [FGF]4 and Activin A) and day 6 (D6) (3 days of pretreatment with FGF4 and Activin A, and 3 days of treatment with hepatocyte growth factor [HGF], FGF1, FGF4, oncostatin M [OsM], dexamethasone [Dex], insulin-transferrin-selenium [ITS], dimethyl sulfoxide [DMSO], and nicotinamide) (■). Undifferentiated adipose-derived stem cells (ASC) (D0) (▒). Data were analyzed by the Pair Wise Fixed Reallocation Randomization Test©, $n = 3$. $^*P < 0.05$). (b) Morphological features of ASC-derived hepatocyte-like cells of ASC derived from Donor #1, Donor #2, and commercially available ASC012202.

in Figure 3(a), changes in the morphology of ASC-derived hepatocyte-like cells (Donor #2) at days 0, 4, 9 and 16 of hepatogenic induction indicate hepatocyte maturation. At day 13, ASC-derived hepatocyte-like cells expressed albumin (Fig. 3b), which was detected by immunostaining, using anti-human specific antibody. Undifferentiated ASC, however, did not express albumin (data not shown). We also checked the functionality of ASC-derived hepatocyte-like cells. Figure 3(c) represents the albumin production at days 3, 6 and 9 of the induction process. ASC-derived hepatocyte-like cells also revealed an ability to uptake low-density lipoprotein (LDL) and store glycogen (Fig. 4).

Transplantation of ASC-derived hepatocyte-like cells into mice with liver injury

To address whether ASC reveal therapeutic abilities to regenerate an injured liver, we transplanted ASC-derived hepatocyte-like cells of Donors #1 and #2 into nude mice with acute liver failure. CCl_4 injury generated oxidative stress and hepatocyte necrosis. Twenty-four hours after CCl_4 injection, mice revealed serious liver injury. Biochemical parameters such as ALT, AST, UA and ammonia were increased in mice with CCl_4 injury compared with non-injured mice (Fig. 5). We transplanted 1.5×10^6 cells of ASC-derived hepatocyte-like cells into a CCl_4-injured mouse. After transplantation, ALT and AST were significantly decreased to a value more than 50% lower than in non-transplanted and injured mice (Fig. 5). Likewise, ammonia concentration was significantly decreased after ASC-derived hepatocyte-like cell transplantation. UA, a marker of oxidative stress, was significantly decreased up to a normal level after transplantation of ASC-derived hepatocyte-like cells (Fig. 5). Hematoxylin-eosin staining revealed that the level of injury was the same in the injured, non-transplanted mice (Fig. 6b,e) as well as in the injured transplanted mice (Fig. 6c,f), in contrast to the non-injured non-transplanted mice (Fig. 6a,d). Significant morphological changes between those mice, however, were detected in the hepatocytes of the non-necrotic area. The